Renewable Integrated Grid Network towards Sustainability – A Study on the Stability Issues

Anulekha Saha^a, Surachai Chaitusaney^a, Aniruddha Bhattacharya^b

^aPower System Research Laboratory, Chulalongkorn University, Bangkok 10330, Thailand ^bDepartment of Electrical Engineering, National Institute of Technology Durgapur, 713209, India

Corresponding Author – Surachai Chaitusaney surachai.c@chula.ac.th

Abstract:- Energy derived from renewable sources in modern times has paved the way towards a sustainable and greener future. Although renewable energy is undisputedly the answer towards decarbonisation, there are certain challenges that need to be overcome before we can completely do away with the use of fossil fuels for power generation. Integrating renewable energy sources into power systems introduces inherent variability to electricity generation, creating a need for robust strategies to ensure system stability. This article addresses one of these challenges by developing a customized security-constrained probabilistic optimal power flow framework tailored for integrated renewable energy systems. The model incorporates solar and wind energy resources through the Two Point Estimate (2m-PEM) method, improving its accuracy and practicality. To enhance the effectiveness of this framework, two advanced evolutionary algorithms, specifically the Fox Inspired Optimization and Coronavirus Herd Immunity Optimizer, are utilized to identify optimal parameter settings for specific objectives. The results demonstrate the model's ability to maintain transient stability even in scenarios where fault clearing times are significantly extended. This study makes a significant contribution to the secure integration of renewable energy sources into power systems. It offers valuable insights into improving transient stability by employing a sophisticated combination of probabilistic optimization and evolutionary algorithms. These findings pave the way for a robust integration of renewable energy while adhering to the stringent stability requirements of modern power systems.

Keywords: critical clearing time, optimal power flow, transient stability, renewable energy.

1. Introduction

Contemporary power systems are meticulously engineered to operate both efficiently and economically. However, the ever-increasing demands on these systems, coupled with the dynamic nature of network characteristics, can potentially introduce instability into the existing infrastructure. To mitigate this challenge, optimal power flow (OPF) emerges as a crucial tool in optimizing the utilization of the power system's capabilities.



An OPF model is designed with the primary objective of minimizing operational costs while adhering to various operational constraints. This entails identifying the optimal operating conditions for generators within the system.

Nome	enclature				
J	Objective Function	θ_{ij}	Phase angle difference of voltages at the i th and j th buses of line i - j	c ₁	Probability of hunting while jumping in north eastern direction with value 0.82
m	Vector of dependent variable	NBU	Total number of buses in the system	c ₂	Probability of hunting while jumping in other direction with value 0.18
n	Vector of independent variable	c	Set of variables of the deterministic OPF problem	M	Minimum time variable
P _{Gen}	Real power output of generator bus	δ	Rotor angle	tt	Minimum time average
P _{Load}	Real power demand of load bus	M	Inertia constant	a	Variable used to control search space
V _{Gen}	Generator bus voltage	N G	Number of generators	B	Best solution
V _{load}	Load bus voltage	p_{n1} ,	Locations (specified values of random variables in the input)	M	Maximum number of iterations
Q_{Gen}	Reactive power delivered by generator	E(Y)	First moments of the output variable	f (Objective function or immunity rate of individual
Q_{Load}	Reactive power demand of load bus	$E(Y^2)$	Second moments of the output variable	x	Gene or decision variable in CHIO
Q_{Com}	Shunt VAR compensator output	φ_{p_n}	Skewness	lb	Lower and upper bounds of x
S _{Load}	Transmission line loading	$\zeta_{p_{n,h}}$	Standard locations	p	CHIO population dimension (number of control parameters)

T	Transformer tap setting	$W_{n,l}$ Weight factor	H . Population size of CHIO
PQ	Total number of load buses	Dist_S_1 Distance of sound travel	x^{ϵ} Infected case
PV	Total number of generator buses	<i>Sp_</i> . Speed of sound in air	Status vector
TL	Total number of transmission lines	Tim Sound travel time, a random number in the range [0,1]	x^{n} Susceptible case
NC	Total number of compensators	Dist_Fox_P 1 Distance of FOX from prey	x^i Immune case
NT	Total number of transformer taps	BestPosition Best search agent	Δj Average of population immunity rates
k	Equality constraint	it Number of iterations	M Maximum infected cases age
l	Inequality constraint	Jump _{it} Jump height	a ₁ Cost coefficients of k th generator
G_{ij}	Conductance of line i - j	t Average time of sound travel	G ₁ Conductance of line m connecting two buses
B_{ij}	Susceptance of line i - j	$X_{(it+1)}$ New position of red FOX	θ_i Phase angle difference between two buses
ref	Deference voltage	magnitude at ith load bus (1 p.u.)

 V_i^{ref} Reference voltage magnitude at ith load bus (1 p.u.)

In addition to cost minimization, the OPF problem also encompasses other vital objectives such as the reduction of voltage deviation, transmission losses, and the enhancement of voltage stability indices. These multifaceted goals collectively contribute to the effective and secure operation of modern power systems. Addressing the optimal power flow (OPF) problem through conventional methodologies proves to be intricate due to the nonlinearity and lack of convexity exhibited by electrical power flow equations with respect to the system's physical variables.

Classical optimization techniques encounter limitations when dealing with objective functions that lack differentiability and/or continuity within the problem's nonlinearity. Considering the inherent nonlinearity of OPF, the adoption of metaheuristic algorithms becomes crucial for adeptly navigating and optimizing this intricate problem [1-5]. The literature offers a host of heuristic algorithms that proficiently tackle the fundamental OPF problem which are Differential Evolution, Hybrid Evolutionary Programming, Tabu Search, Bacteria Foraging, Gravitational Search, and Particle Swarm Optimization [6-13]. Moreover, several Pareto-based multiobjective optimization strategies have demonstrated efficacy in resolving multi-objective OPF (MOPF) issues. These approaches encompass methods such as Quasi-Oppositional Teaching Learning Based Optimization, Biogeography-Based Optimization, Harmony Search Algorithm, and Symbiotic Organisms Search Algorithm, facilitating the identification of optimal solutions that strike a balance among conflicting objectives [14-19].

As the power system evolves to accommodate the dynamic inputs from renewable sources, the formulation of the probabilistic optimal power flow (POPF) problem gains complexity, necessitating innovative approaches to ensure secure and efficient operation. The stochastic variability of renewable generation necessitates the development of a probabilistic OPF framework to appropriately account for uncertainties introduced by renewable energy sources (RESs). The confluence of renewable generation and power electronics technologies enables effective integration, resulting in the emergence of diverse control strategies [20–21] and optimization techniques [22–23] tailored to augment system stability and efficiency.

However, the seamless integration of renewable resources demands a deeper consideration of system contingencies to ensure safe operation. Unforeseen disturbances, with regard to load fluctuations, line switching, line-to-ground faults, and unexpected outages, can propel the system into transient instability conditions, characterized by significant rotor angle deviations. Addressing these challenges mandates not only the minimization of the objective function but also the meticulous management of transient stability. While conventional OPF strategies excel in maintaining voltage stability under normal conditions, they often fail in guaranteeing transient stability during fault events. To effectively safeguard system stability in the face of such adversities, it becomes imperative to introduce an additional constraint pertaining to transient stability within the context of the probabilistic OPF formulation, thereby giving rise to transient stability constrained probabilistic optimal power flow (TSC-POPF) model. By amalgamating the probabilistic treatment of renewable uncertainty with the consideration of transient stability, this research endeavours to holistically address the multifaceted challenges arising from the integration of renewable energy sources within the power system framework.

Diverse methodologies have been proposed in the literature to tackle distinct aspects of power system optimization. Specifically, the probabilistic optimal power flow (POPF) problem and the transient stability-constrained optimal power flow (TSC-OPF) problem have been addressed through separate approaches. Various techniques have emerged to address the probabilistic OPF problem, including Monte Carlo simulation (MCS), point estimate methods, first-order second moments, and the Cumulant method [24 - 30]. However, MCS suffers from computational inefficiency due to prolong processing times. Meanwhile, the Cumulant method becomes progressively intricate as the number of variables increases in POPF analyses. To mitigate these challenges, a promising alternative is the Two-Point Estimate Method (2m PEM).

The TSC-OPF problem has also attracted considerable attention in the literature [31 - 33]. One approach utilized the Chaotic Artificial Bee Colony algorithm [31], while another introduced a single machine equivalent (SIME) technique [32] that efficiently managed transient stability without involving complex sets of differential algebraic equations.

Research Gaps and Proposed Methodology

As observed in the literature, the SIME method's reliance on approximations and its inability to optimize generation shifts limit its optimality. In this context, the transient stability constraint (TSC) is quantified as rotor angle deviations from the center of inertia frame, using Taylor series expansion of differential equations [34]. Particle swarm optimization (PSO) was employed in [35] to minimize costs while satisfying TSC-OPF constraints. Additionally, [36] presented two distinct techniques for TSC-OPF resolution: one involving the generators' maximum relative rotor angle deviations (RRAD) as a constraint and another based on generator power outputs. Metaheuristic algorithms, such as oppositional krill herd, chaotic whale optimization, hybrid symbiotic search, and group search optimization, have demonstrated promise in effectively addressing the TSC-OPF problem by adhering to system constraints without compromising accuracy [38 - 43]. Notably, a strategy dividing the system into coherent sections was proposed in [37] for faster TSC-OPF resolution.

In this paper, we introduce novel methodologies for addressing the TSC-OPF problem, avoiding the limitations associated with the SIME method [43]. Our approach leverages the RRAD constraint to enhance transient stability in the system. In this study, we introduce an innovative TSC-OPF model with renewable energy integration. We leverage the 2PEM [44] to effectively model the inherent uncertainty associated with renewable energy source (RES) generation. To assess the performance and robustness of our model, we employ two cuttingedge metaheuristic algorithms: Fox Inspired Optimization (FOX) [45] and Coronavirus Herd Immunity Optimizer (CHIO) [46]. These algorithms are evaluated using the IEEE 30 bus system [47], [48]. We benchmark our results against those presented in [50] to estimate the annual savings in generation cost.

Contributions of the Article

Our study formulates the probabilistic aspect of the OPF problem by employing 2m PEM. This approach accounts for the uncertainties in RES outputs by representing each uncertain variable with two deterministic values adjoining its mean value. Consequently, for every n uncertain variable, we necessitate 2n runs of deterministic OPF.

The principal contributions of this paper encompass:

- The introduction of 2m PEM-based POPF model.
- The extension of the 2m PEM-based POPF model to incorporate TSC.
- The utilization of two state-of-the-art algorithms, FOX and CHIO, to solve the designed problem.

Section 2 elucidates the formulation of the TSC-POPF problem and provides an abridged explanation of the 2m PEM technique. Section 3 furnishes a comprehensive overview of the FOX and CHIO algorithms as applied to the TSC-POPF problem. In Section 4, we define the objective functions and delineate the test system in Section 5, while Section 6 presents an exhaustive analysis of our results, followed by the conclusion.

The algorithms are tested using the IEEE 30 bus system, scrutinizing various objectives for different fault clearing times. Our findings underscore the efficacy of the proposed TSC-POPF model in achieving optimal outcomes while ensuring transient stability within the system across all scenarios examined.

2. Mathematical Formulation

This section presents an exhaustive mathematical formulation of the proposed problem.

Formulation of the TSC-OPF Problem

A deterministic OPF model identifies the best settings for network parameters to minimize certain objectives after meeting different equality and inequality criterions. The deterministic OPF problem is mathematically formulated and described below:

$$min J(m, n)$$
 (1)

Subject to
$$k(m, n) = 0$$
 (2)

and
$$l(m,n) = 0$$
 (3)

m constitutes the slack bus power P_{Gen1}, V_{Load}, Q_{Gen}, and S_{Load} and can be stated as:

$$m^T = [P_{Gen1}, V_{LoadPO}, Q_{Gen1}, \dots Q_{GenPV}, S_{Load1}, \dots S_{LoadTL}]$$

1243

Revised: 15-05-2024 Received: 06-04-2024 Accepted: 28-06-2024

n constitutes P_{Gen} (except slack bus), V_{Gen}, Q_{Comp}, T_i and can be stated as:

$$n^{T} = \left[P_{Gen2}, \dots P_{GenPV}, V_{Gen1}, \dots V_{GenPV}, Q_{Comp1}, \dots Q_{CompNC}, T_{1}, \dots T_{NT} \right]$$

$$(5)$$

Equality constraints' set k denotes load flow equations, which are expressed as shown below:

$$P_{Geni} - P_{Loadi} = V_i \sum_{j=1}^{NBUS} V_j (G_{ij} cos\theta_{ij} - B_{ij} sin\theta_{ij})$$
 (6)

where, i=1,2,3,....NBUS.

$$Q_{Geni} - Q_{Loadi} = V_i \sum_{j=1}^{NBUS} V_j (G_{ij} cos\theta_{ij} + B_{ij} cos\theta_{ij})$$
(7)

where, i = 1, 2, 3,NBUS.

Inequality constraints' set 1 is comprised of lower and upper limits on generator (considers limits on PV bus voltages and P_{Gen} and Q_{Gen}), transformer (limits of the T), shunt reactive compensator (limits on Q_{comp}) and security constraints (limit on the PQ bus voltages and the line loadings) by the following equations:

$$V_{Geni}^{min} \le V_{Geni} \le V_{Geni}^{max} \tag{8}$$

$$P_{Geni}^{min} \le P_{Geni} \le P_{Geni}^{max} \qquad \qquad i = 1, 2, \dots, PV$$
 (9)

$$P_{Geni}^{min} \le P_{Geni} \le P_{Geni}^{max} \qquad i = 1, 2, ..., PV$$

$$Q_{Geni}^{min} \le Q_{Geni} \le Q_{Geni}^{max} \qquad (10)$$

$$T_i^{min} \le T_i \le T_i^{max} \qquad i = 1, 2, \dots, NT$$
 (11)

$$Q_{Compi}^{min} \le Q_{Compi} \le Q_{Compi}^{max} \qquad i = 1, 2, \dots, NC$$
(12)

$$V_{Loadi}^{min} \le V_{Loadi} \le V_{Loadi}^{max} \qquad i = 1, 2, \dots, PQ \tag{13}$$

$$S_{Loadi}^{min} \le S_{Loadi} \le S_{Loadi}^{max} \qquad i = 1, 2, \dots, TL$$
 (14)

For the system to be able to handle fault conditions, we must incorporate TSC into our OPF problem apart from constraints given by (8) - (11) and (13) - (14). TSC is defined as modulus of the maximum allowed difference between rotor angles and initial centre of the generators [31]:

$$100 \le |\partial - \partial_{COI}| \le 180^{\circ} \tag{15}$$

where,
$$\partial_{COI} = \frac{\sum_{p=1}^{NG} M_p \partial_p}{\sum_{p=1}^{NG} M_p}$$
 (16)

where, ∂_p is rotor angle, M_p is inertia constant of p^{th} generator.

RRADs must not go beyond 180° , as per [34 - 35] in order to ensure a transiently stable system.

Formulation of Wind and Solar Power Generation

The probability of wind speed in w m/s is obtained from the Weibull distribution for a given shape factor k and scale factor c as follows [51]:

$$f_w(w) = \left(\frac{k}{c}\right) \left(\frac{w}{c}\right)^{(k-1)} e^{-(w/c)^k} \quad \text{for } 0 < w < \infty$$
 (17)

Mean of the Weibull distribution is obtained as:

$$Mean_{wbl} = c * \mathbb{F}(1+1/k) \tag{18}$$

Two identical wind generators are placed at bus 26 and 30. Details of wind generator are provided in Table 1 below:

Table 1: Weibull probability distribution parameters for stochastic wind power generation.

Wind		Rated	Shape	Scale
Power	Bus No.	Power	Parameter	Parameter
Generator		(kW)	(k)	(c)
1, 2	26, 30	200	2	15

The power output (p_w) of the wind turbines vary with wind speed and are according to the following equation:

$$p_{w}(w) = \begin{cases} 0 & for \ w < w_{in} \ or \ w > w_{out} \end{cases}$$

$$p_{wr} \left(\frac{w - w_{in}}{w_{r} - w_{in}}\right) & for \ w_{in} \le w \le w_{r}$$

$$p_{wr} & for \ w_{r} \le w \le w_{out}$$

$$(19)$$

The cut-in speed (w_{in}) is 2.5 m/s, rated speed (w_r) is 11.5 m/s, cut-out speed (w_{out}) is 20 m/s, and rated power (p_{wr}) is 200 kW according to the Hummer wind turbine model datasheet of [53].

The solar irradiance (G_s) probability is represented using the Lognormal probability distribution function [52] as shown:

$$f_S(G_S) = \left(\frac{1}{G_S \sigma \sqrt{2\pi}}\right) e^{\left\{-(\ln G_S - \mu)^2 / 2\sigma^2\right\}} \quad \text{for } G_S > 0$$
 (20)

Here μ and σ represent respectively the mean and standard deviation.

The probability parameters for solar units are given in Table 2:

Table 2: Solar parameters for Lognormal probability distribution.

Solar PV Bus No. Power
$$(MW)$$
 Mean (μ) Standard Deviation (σ) 1, 2 10, 12 10 5.2 0.6

Solar irradiance gets converted to energy as per the following equation [53]:

$$P_{solar}(G_s) = \frac{(P_{solar} * G_s^2)}{(G_{standard} * G_{cert})} \quad \text{for } 0 < G_s < G_{cert}$$

$$= \frac{(P_{solar} * G_s)}{G_{standard}} \quad \text{for } G_s \ge G_{cert} \quad (21)$$

Here, $G_{standard}$ is solar irradiance under standard environmental considerations and is $1000 \, W/m^2$. G_{cert} is a particular irradiance point.

Modeling TSC-POPF Problem using 2m PEM Method

In addressing the formidable challenges posed by the probabilistic nature of renewable energy generation, our chosen methodology involved the utilization of the 2m PEM. Initially proposed by Rosenblueth [28], PEM serves as a valuable technique for approximating and managing uncertainties within power systems. However, it is not without its limitations, particularly when dealing with variables that exhibit symmetry. In response to this limitation, Hong [29] introduced an enhanced variant of PEM. This upgraded approach significantly enhances computational efficiency and expands its applicability, making it particularly adept at handling probabilistic aspects effectively.

POPF function, denoted as Y, can be mathematically expressed as follows [26]:

$$Y = f(X) (22)$$

where, X constitutes the input variables. Uncertain variable set m consists of the outputs from wind and solar sources. The equation presented above can be expressed in the following form:

$$Y = f(c, p_1, p_2 \dots p_m) \tag{23}$$

Initial central moments, such as mean, variance, and skewness, provide the statistical data needed in 2m PEM for the uncertain variables. We need to calculate (23) 2m times for each of the moments in the following manner:

$$Y(n,h) = f(c, \mu_{p1}, \mu_{p2}, \dots, p_{n,h}, \dots, \mu_{pm}); \text{ where, } h = 1,2; n = 1,2...m$$
 (24)

Once the deterministic OPF solution is obtained, (24) is calculated, to obtain mean (μ_{pn}) and standard deviation (σ_{pn}) . Steps to calculate moments with 2m PEM for TSC-POPF problem is demonstrated below:

Step 1: Randomly generate m input variables.

Step 2: Fix first, second moments of output variable to zero i.e, E(Y) = 0 and $E(Y^2) = 0$.

Step 3: For each p_n , calculate φ_{p_n} as follows:

$$\varphi_{p_{n,3}} = \frac{E[p_n - \mu_{p_n}]}{(\sigma_{p_n})^3} ; \qquad n = 1, 2, 3, ..., m$$
(25)

Step 4: Calculate two standard locations as follows:

$$\zeta_{p_{n,h}} = \frac{\varphi_{p_{n,3}}}{2} + (-1)^{3-h} \sqrt{\left(m + \left(\frac{\varphi_{p_{n,3}}}{2}\right)^2\right)}$$
 (26)

Step 5: Compute two estimated locations (ELs) of each variables:

$$p_{n,h} = \mu_{p_n} + \zeta_{p_{n,h}} \cdot \sigma_{p_n}$$
 ; $h = 1,2$ (27)

Step 6: Compute deterministic OPF using (24) for these ELs.

Step 7: Calculate two weighting factors for p_n as follows:

$$W_{n,h} = \frac{(-1)^h}{m} \cdot \frac{\zeta_{p_{n,3-h}}}{\zeta_{p_{n,1}} - \zeta_{p_{n,2}}} \qquad ; \qquad h = 1,2$$
 (28)

Step 8: For output random variable, evaluate first, second moments as shown:

$$E(Y^k) = \sum_{n=1}^m \sum_{h=1}^2 \left(W_{n,h} \cdot \left(Y_{n,h} \right)^k \right) \; ; k = 1,2$$
 (29)

Step 9: Redo steps 3 - 8 for every uncertain parameter.

Step 10: Evaluate μ and σ as shown:

$$\mu = E(Y^1)$$
 ; $\sigma = \sqrt{E(Y^2) - \mu^2}$ (30)

This formulation enables us to effectively account for the probabilistic aspects of renewable energy generation within the optimal power flow framework, thus contributing to a more reliable and stable power system operation.

3. Application of Evolutionary Algorithms to the Proposed TSC-POPF Problem

Given the inherent limitation of classical optimization methods, characterized by their susceptibility to converging towards local optima, our approach to tackling the TSC-POPF problem involves the utilization of evolutionary algorithms. The primary motivation behind this strategy is to enhance the likelihood of obtaining superior solutions. In this section, we present a concise overview of the two evolutionary algorithms that have been employed to tackle the TSC-POPF problem, focusing on their role in minimizing the objective function values.

FOX optimization algorithm [45]

The FOX algorithm draws inspiration from the natural hunting behaviors of red foxes. This bio-inspired algorithm is founded on the intricate techniques employed by red foxes in estimating distances to their prey, ultimately ending in successful hunts. The hunting process of red foxes in snowy environments serves as the foundational concept for the FOX algorithm, which can be outlined as follows:

- i. Randomized Search Initiation: In response to the diminished visibility caused by snow cover, red foxes initalize their search for prey in a random manner. This randomness in the initial search pattern mirrors the exploratory phase of the FOX algorithm.
- ii. Prey Location Prediction: Red foxes employ their acute hearing capabilities to detect and focus on the ultrasonic emissions emitted by their prey. This auditory data aids them in predicting the probable location of the prey. In parallel, the FOX algorithm incorporates this predictive aspect, seeking to approach the optimal solution.

- iii. Distance Estimation via Echo: By actively listening to the reflected ultrasounds and precisely measuring the time difference between emission and reception, the red fox skillfully estimates its distance from the prey. This echolocation strategy serves as a heuristic for the FOX algorithm to gauge the proximity to a potential solution.
- iv. Jump Calculation: Upon reaching a sufficiently close distance to the prey, the red fox calculates the optimal jump required to effectively capture its target. In the algorithmic context, this step corresponds to refining the search process as it converges towards the solution.
- v. Optimized Random Walk: The red fox performs random movements, precisely calculated to optimize both time and positioning for the final pounce on the prey. Similarly, the FOX algorithm incorporates a controlled randomization process to iteratively refine its search, striving for improved solutions.

By imitating these inherent behaviors of red foxes, the FOX algorithm encapsulates a nature-inspired approach to optimization, potentially overcoming the local optima issues often encountered by classical optimization techniques.

In the literature [49], it has been empirically demonstrated that executing jumps in the northeast direction significantly augments a Fox's probability of successfully capturing its prey, resulting in an impressive success rate of 82%. Conversely, jumps in the opposite direction have been observed to diminish this success rate to a mere 18%. To strike a balance between the critical aspects of exploitation and exploration, the algorithmic iterations are evenly partitioned. This strategic allocation of iterations serves as a preventative measure, guarding against the algorithm becoming trapped in local optima.

The phases of the algorithm are described as follows:

Exploitation

The probability of achieving a successful kill is determined by a stochastic variable denoted as p, which is constrained to the interval [0,1]. In scenarios where the calculated value of p exceeds the threshold of 0.18, the red fox initiates a relocation process as shown in the following steps:

$$Dist_S_T_{it} = Sp_S * Time_S_T_{it}$$
(31)

where,
$$Sp_S = BestPosition_{it}/Time_{S_{T_{it}}}$$
 (32)

Distance of FOX from its prey is calculated as:

$$Dist_Fox_Prey_{it} = Dist_S_T_{it} * 0.5$$
(33)

After estimating the distance, the fox makes a jump to catch the prey. This jump is calculated as follows:

$$Jump_{it} = 0.5 * 9.81 * t^2 (34)$$

The value 9.81 represents acceleration due to gravity. New position of red Fox when it jumps in the north eastern direction is dictated by its probability of catching prey, which is 82 %. The new position is calculated as follows:

$$X_{(it+1)} = Dist_Fox_Prey_{it} * Jump_{it} * c_1$$
(35)

If the FOX jumps in other directions, the probability of catching prey drops to 18% and its position is calculated as:

$$X_{(it+1)} = Dist_Fox_Prey_{it} * Jump_{it} * c_2$$
(36)

Exploration

In this phase, the fox walks randomly in search of prey in the search area based on the latest best position obtained as follows:

$$X_{(it+1)} = BestX_{it} * rand(1, dimension) * MinT * a$$
(37)

where,
$$MinT = Min(tt)$$
 (38)

where,
$$tt = sum(Time_S_T_{it}(i,:))/dimension$$
 (39)

and,
$$a = 2 * (it - (1/Max_it))$$
 (40)

FOX algorithm applied to TSC-POPF

This section provides the flowchart representation of the FOX algorithm as applied to TSCP-OPF problem in Fig. 1. Case studies done in this paper considered the following parameter values:

 $r = rand(0,1); p = rand(0,1); 0.19 < c_1 < 1; 0 < c_2 \le 0.18; Max_{it}$ = 100; SearchAgents = 30.

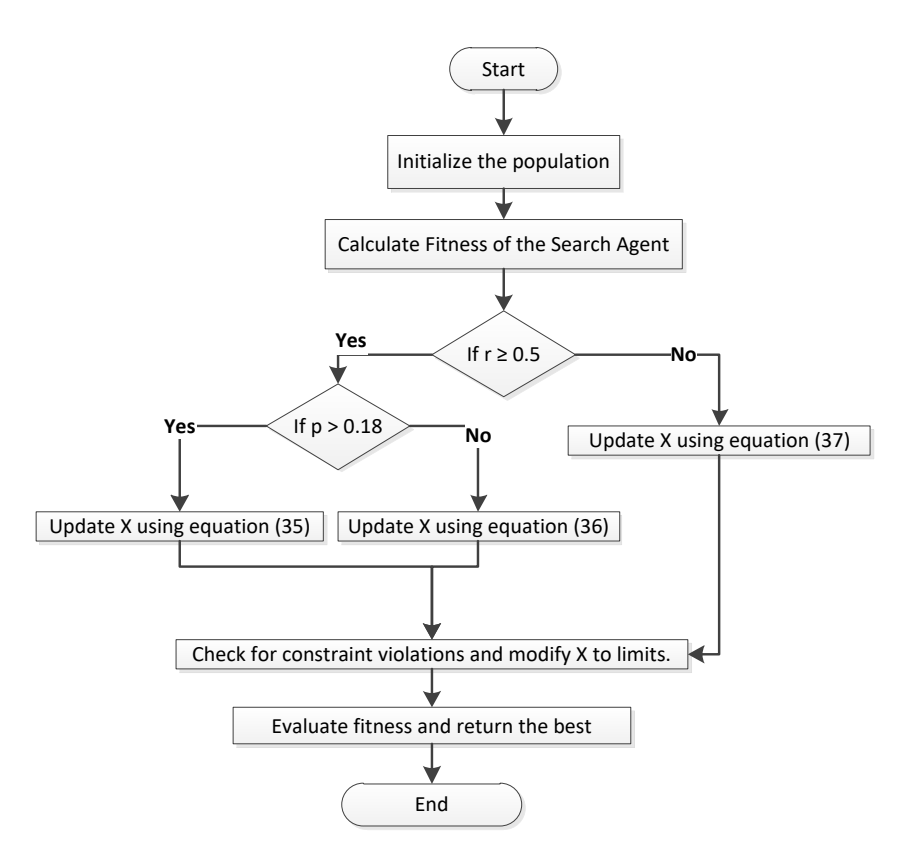


Fig. 1. Flowchart for FOX algorithm.

Coronavirus herd immunity optimization (CHIO) [46]:

CHIO stands as an evolutionary algorithm, crafted in response to the COVID-19 pandemic, drawing inspiration from the principles of herd immunity and social distancing [46]. Herd immunity characterizes a scenario wherein a substantial segment of the population attains immunity against the disease, resulting in a notable reduction in transmission rates. The achievement of herd immunity is intrinsically tied to factors encompassing the susceptible, infected, and immune proportions within the population concerning COVID-19. The population's dynamic evolution is fundamentally influenced by the strategic implementation of social distancing measures.

The governing parameters within the CHIO framework incorporate the basic reproduction rate, signifying the velocity of virus transmission amongst individuals, and the maximum age of infected cases, which classifies these cases based on their recovery or fatality statuses.

The following steps are involved in the designing of CHIO algorithm:

Initialization of CHIO parameters for the optimization problem

The CHIO problem is framed for a given objective function as follows [46]:

$$\min f(x) : x_i \in [lb_i, ub_i] \tag{41}$$

where,
$$x_i = (x_1, x_2, x_3, \dots x_p)$$

3.2.2. Generation of herd immunity population (HIP)

The HIP is generated as follows:

$$HIP = \begin{vmatrix} x_1^1 & x_2^1 & \cdots & x_p^1 \\ x_2^1 & x_2^2 & \cdots & x_p^2 \\ \cdots & \cdots & \vdots & \cdots \\ x_1^{HIS} & x_2^{HIS} & \cdots & x_p^{HIS} \end{vmatrix}$$
(42)

3.2.3. Herd immunity evolution

Here, the genes get updated based on three rules according to BR_r (basic reproduction rate) as shown:

$$\begin{aligned} x_i^j(it+1) &= x_i^j(it) & r \geq BR_r \\ &= C\left(x_i^j(it)\right) & 0 < r < \left(\frac{1}{3} \times BR_r\right) & \text{(Infected)} \\ &= N\left(x_i^j(it)\right) \left(\frac{1}{3} \times BR_r\right) < r < \left(\frac{2}{3} \times BR_r\right) & \text{(Susceptible)} \\ &= R\left(x_i^j(it)\right) & \left(\frac{2}{3} \times BR_r\right) < r < BR_r & \text{(Immune)} \end{aligned}$$

$$C\left(x_i^j(it)\right) = x_i^j(it) + r \times (x_i^j(it) - x_i^c(it)) \tag{44}$$

 $x_i^c(it)$ is selected at random from any infected case x^c depending on S such that $c = \{i | S_i = 1\}$.

$$N\left(x_i^j(it)\right) = x_i^j(it) + r \times (x_i^j(it) - x_i^m(it)) \tag{45}$$

 $x_i^m(it)$ is selected randomly from any susceptible case x^m depending on S such that $m = \{i | S_i = 0\}$.

$$R\left(x_i^j(it)\right) = x_i^j(it) + r \times (x_i^j(it) - x_i^v(it)) \tag{46}$$

 $x_i^{\nu}(it)$ is selected randomly from any immune case x^{ν} depending on S such that:

$$f(x^{v}) = \arg_{j \sim \min_{\{k \mid S_{v} = 2\}}} f(x^{j})$$
(47)

The age vector A_i is increased by 1 if $S_i = 1$.

 S_i gets updated in every case depending on herd immune threshold utilizing the equation:

$$S_{j} = 1 \qquad f\left(x^{j}(it+1)\right) < \frac{f(x)^{j}(it+1)}{\Delta f(x)} \wedge S_{j} = 0 \wedge is_{corona\left(x^{j}(it+1)\right)}$$

$$= 2 \qquad f\left(x^{j}(it+1)\right) > \frac{f(x)^{j}(it+1)}{\Delta f(x)} \wedge S_{j} = 1 \qquad (48)$$

where, $is_Corona(x^j(it+1)) = 1$ when $x^j(it+1)$ gets a value from infected case and $\Delta f(x) = \sum_{i=1}^{HIS} f(x_i) / HIS$.

If this evolved population is well immune to COVID-19, then the herd attains immunity threshold.

3.2.4. Fatality cases

In case, the immunity rate $f\left(x^{j}(it+1)\right)$ of the present infected case does not get better for some iterations, which is equal to value of Max_Age , (i.e., $A_{j} \ge Max_Age$), then this infected case is considered dead. This case is then generated again for all control parameters.

3.2.5. CHIO algorithm applied to TSCP-OPF problem

Case studies done in this paper considered the following parameter values:

$$BR_r = 0.001, Max_{Age} = 100, HIS = 30, Max_{it} = 100.$$

The flowchart of the CHIO algorithm is provided below in Fig. 2.

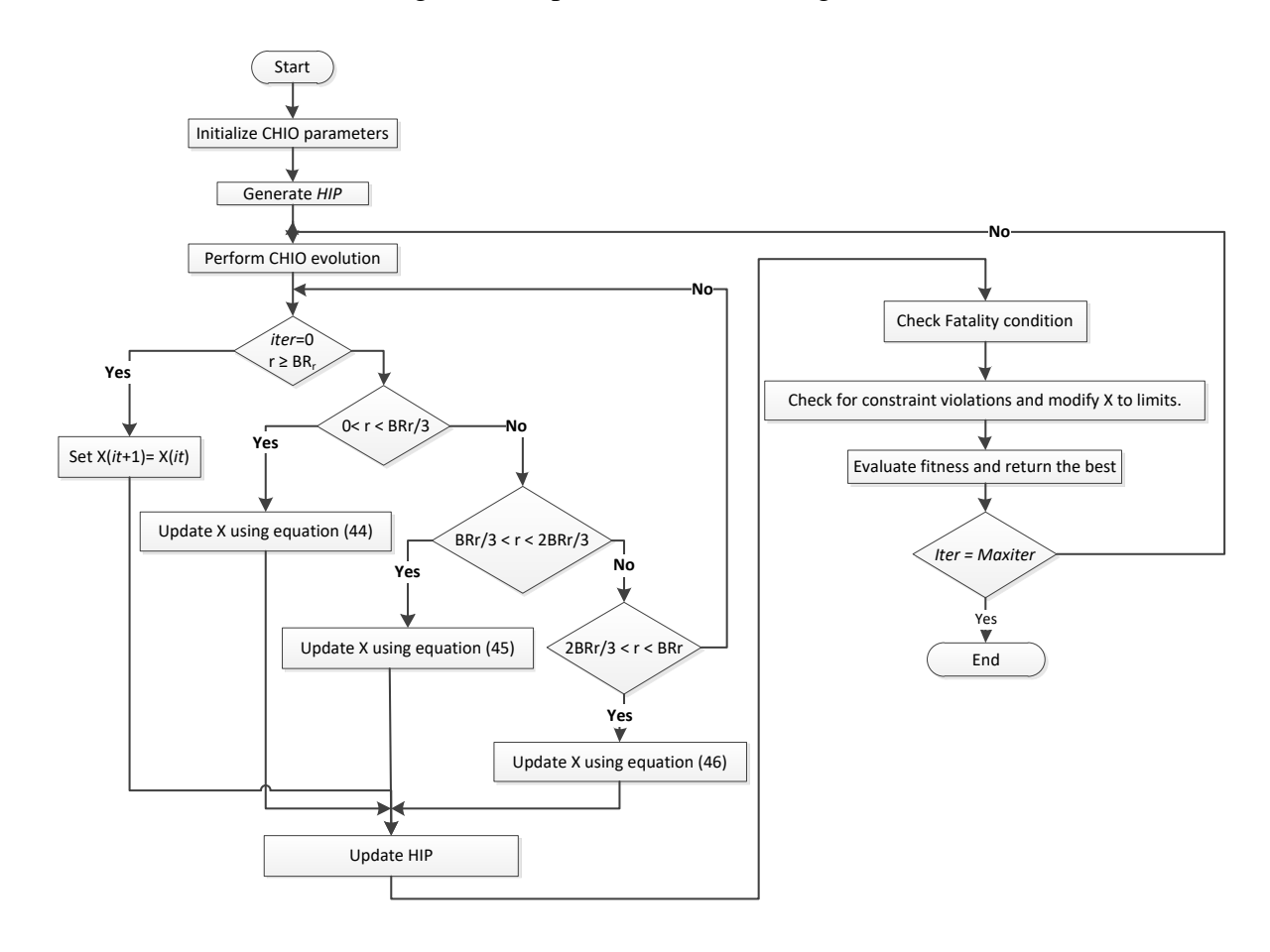


Fig. 2. Flowchart for CHIO algorithm.

4. Objective Functions of TSC-POPF Problem

This section presents the objective functions studied using the proposed system, to which, FOX and CHIO are applied.

4.1. Generation Cost Minimization

The objective of minimizing electricity generation costs can be explicitly defined with respect to the real component of the output power in the following manner:

$$O_1 = min(F(P))$$

$$= min(\sum_{k=1}^{NG} F(P_k)) = min(\sum_{k=1}^{NG} (a_k + b_k P_k + c_k P_k^2))$$
(49)

4.2. Transmission loss minimization

The minimization of real power transmission losses can be explained as follows:

$$O_2 = min(P_L)$$

$$= min(\sum_{m=1}^{TL} G_m(V_i^2 + V_k^2 - 2V_i V_k cos\theta_{ik}))$$
(50)

4.3. Voltage deviation (VD) minimization

$$O_3 = \min(VD) = \min\left(\sum_{i=1}^{TL} \left(V_i - V_i^{ref}\right)\right)$$
 (51)

All the objective functions are minimized using FOX and CHIO algorithms subject to satisfying the constraints of (8) - (11) and (13) - (15).

5. System Description

In this section, we present a concise representation of the system to which our proposed model is applied. The primary focus lies in the minimization of objective functions through the utilization of FOX and CHIO algorithms across various distinct scenarios. To facilitate this process, custom codes were developed in the MATLAB programming environment, and subsequent simulations were executed on a personal computer equipped with an Intel Core i3-3110M CPU, 4 GB of RAM, operating at a clock speed of 2.4 GHz.

IEEE 30 bus system

The system under investigation is the IEEE 30-bus system, as defined in reference [47]. This system comprises 30 buses, 6 generators, 41 transmission lines, and 4 tap-changing transformers. The total load imposed on the system amounts to 189.2 MW and 107.2 MVAr. To perform TSC-POPF operation, the following conditions were established:

- 1) Solar power injection was incorporated at buses 10 and 12, while wind power injection was implemented at buses 26 and 30.
- 2) A single contingency analysis was executed considering a 3 phase fault close to bus 2 (at t=0), which was cleared after taking out line 2 5, similar to the studies carried out in [31], [35] and [40] for the sake of comparison.

6. Results and Discussion

This section presents results obtained after performing different studies on the system for different cases/scenarios and their exhaustive analysis. The following cases were studied for the system:

- Case 1: A baseline investigation was carried out involving a normal OPF analysis without the consideration of renewable generation or TSC.
- Case 2: A probabilistic OPF analysis was performed without the presence of any contingency events.
- Case 3: TSC-OPF was conducted for the system, omitting renewable energy sources, with a specified fault clearing time (CT) of 0.18 seconds.
- Case 4: TSC-POPF analysis was conducted, considering a fault CT of 0.18 s.
- Case 5: The fault CT was extended to 0.49 seconds, and TSC-POPF analysis was subsequently undertaken.

For all cases, the maximum simulation duration was constrained to 5 seconds, with an integration time step of 0.01 seconds. Additionally, RRAD was constrained to 150° for the above cases.

Case 1

In this case, TSC and renewable generation were not considered. For this case, when a 3 phase fault occurred close to bus 2 (at t=0), and was cleared by taking out line 2-5, maximum fault CT was observed as 0.1298 s, beyond which the system became unstable as can be seen in Fig. 3. This is because the system was not subjected to satisfy the TSC in (15).

Table 3 shows the minimized values obtained for O_1, O_2 , and O_3 for Case 1. It can be noted that FOX algorithm performed superior to CHIO for all the objectives. It was able to reduce the generation cost by 0.03%, transmission loss by 5.03% and VD by 11.07% when compared to CHIO.

The convergence characteristics obtained using CHIO and FOX algorithms for all objectives are depicted in Fig. 4. It can be noted that CHIO took lesser iterations to converge as compared to FOX algorithm for all the objective functions. However, FOX was better in minimizing the objective functions.

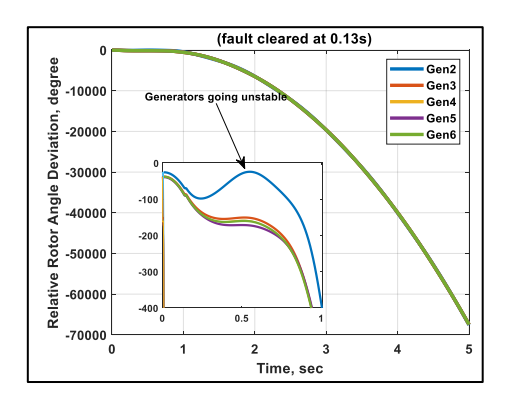


Fig. 3. RRADs for Case 1

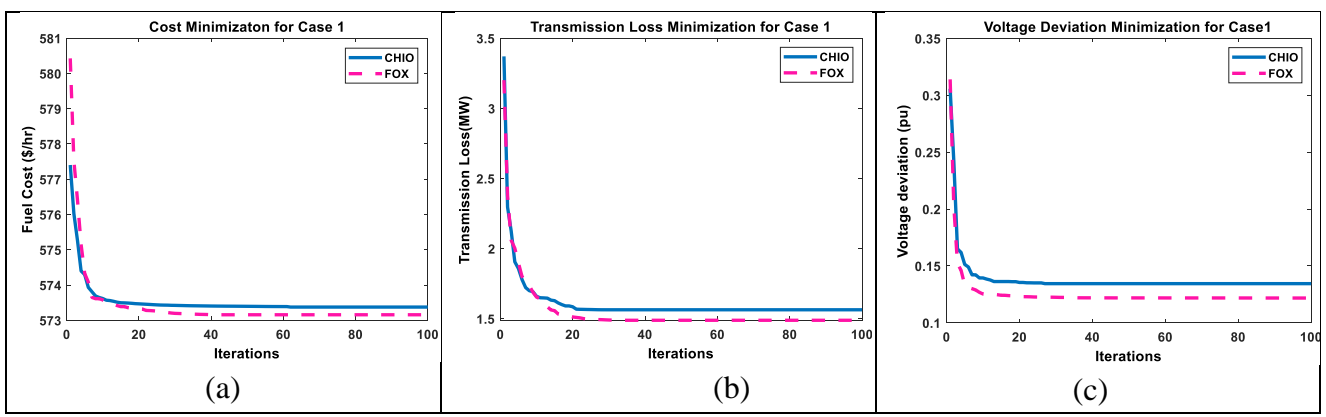


Fig. 4. Convergence characteristics of (a) cost, (b) loss and (c) voltage deviation minimization for Case 1 using CHIO and FOX algorithms.

Table 3: Objective function values using CHIO and FOX Algorithms.

Corresponding	CHIO	FOX	CHIO	FOX	CHIO	FOX
values of other objectives	Cost Minimization		Loss Minimization		Voltage Deviation Minimization	
Cost(\$/h)	573.374 5	573.15 6	640.76 1	637.94 2	600.5971	610.1805
Transmission Loss(MW)	2.1391	2.0818	1.5635	1.4886	2.8921	2.9980
Voltage deviation(p.u.)	1.3756	1.9066	0.4288	0.7805	0.1344	0.1210

Table 4: Comparative Study of Cost Minimization Objective Function for Case 1.

Corresponding values of other objectives	DE[40]	SOS[40]	HSOS[40]	CHIO	FOX
Cost(\$/h)	574.1681	574.0697	573.3098	573.3745	573.1564
Transmission Loss(MW)	2.2700	2.3328	2.1100	2.1391	2.0818
Voltage deviation(p.u.)	0.8821	0.7058	1.6330	1.3756	1.9066

From comparative study of cost minimization objective represented by Table 4, it can be noted that FOX algorithm outperformed all other algorithms in minimizing the generation cost.

Case 2

This case considers probabilistic generation from two solar and two wind generations at bus no.s 10, 12, 26 and 30. Table 5 presents the minimized values for objective functions considered. TSC was not added to this case. We can see great reduction in generation cost, to the extent of 1.23 % for CHIO (annual savings of 61442.64 \$) and 3.4% for FOX algorithm (annual savings of 169039.0292 \$) as compared to Case 1. For the present case, FOX outperformed CHIO again in minimizing generation cost by 2.25%, transmission loss by 1.56% and voltage deviation by 6.12%.

Table 5. Minimization of all Objectives using CHIO and FOX Algorithms for Case 2.

Corresponding	CHIO	FOX	CHIO	FOX	CHIO	FOX
values of	C	ost	Lo	oss	Voltage 1	Deviation
other objectives	Minim	ization	Minim	ization	Minim	ization
Cost(\$/h)	566.36 05	553.859 7	625.280	626.962	661.3079	689.0710
Transmission Loss(MW)	2.2973	2.3324	1.3306	1.3102	5.5782	5.7733
Voltage deviation(p.u.)	1.9804	1.6172	1.9340	1.9953	0.1629	0.1535

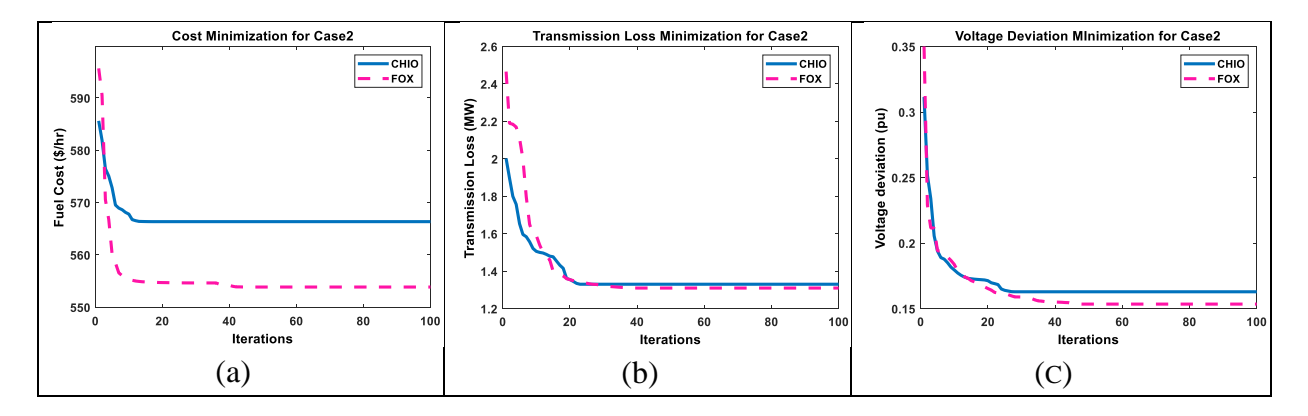


Fig. 5.Convergence characteristics of (a) cost, (b) loss and (c) voltage deviation minimization for Case 2 using CHIO and FOX algorithms.

Fig. 5 presents the convergence characteristics for all objectives using FOX and CHIO. For this case too, CHIO converged slightly faster than FOX, but the latter provided better results.

Case3

For this case, no probabilistic generation was considered. Fault condition was same as in Case 1. Time to clear the fault was considered as 0.18 s after incorporating TSC given in (15).

Table 6. Minimization of all Objectives using CHIO and FOX Algorithms for Case 3.

Corresponding	CHIO	FOX	CHIO	FOX	CHIO	FOX
values of	Co	ost	Lo	OSS	Voltage l	Deviation
other objectives	Minim	ization	Minim	ization	Minim	ization
Cost(\$/h)	574.55 08	574.13 72	635.24 75	638.89 49	635.5991	692.1245
Transmission Loss(MW)	2.4193	2.3276	1.4486	1.3742	5.8458	5.7505
Voltage deviation(p.u.)	0.3695	0.4314	1.3829	1.6892	0.1682	0.1519

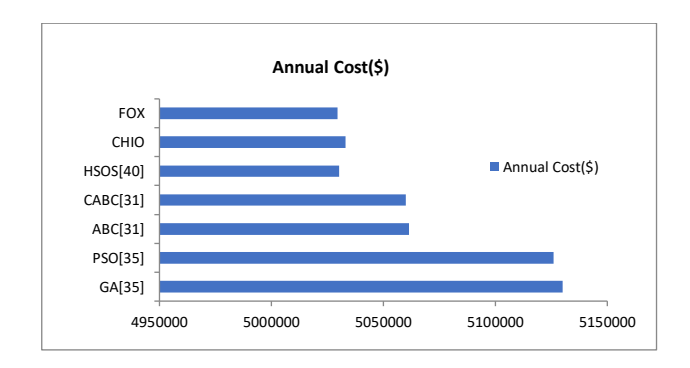


Fig. 6. Annual cost of generation obtained by different algorithms as compared to case 3.

Table 7. Comparative Study of Cost Minimization Objective Function for Case 3.

Comparative sudy (tc=0.18s)							
Corresponding values of	GA[35]	PSO[35	ABC[3	CABC[3	HSOS	СНІО	FOX
other objectives		J	*1	- J			
Cost(\$/h)	585.62	585.17	577.78	577.630	574.22	574.55	574.13
Cost(ϕ/Π)	00	00	00	0	55	08	72
Transmission Loss(p.u)	NA	NA	NA	NA	235.58 00	2.4193	2.3276
Voltage deviation(p.u.)	NA	NA	NA	NA	0.4332	0.3695	0.4314

Table 6 presents the minimization of all objectives for this case and Table 7 presents the comparative study for cost minimization objective. Similar observations regarding performances of CHIO and FOX algorithms are seen for all the objectives with FOX outperforming CHIO. Fig. 6 presents the annual cost of generation in \$ obtained by FOX and CHIO in comparison with other algorithms. It can be observed that application of FOX resulted in the least annual generation cost. Annual savings obtained by FOX as compared to other algorithms are shown in Table 8.

Table 8. Annual Savings in Generation Cost for Case 3.

Algorithm	GA[35]	PSO[35]	ΔRC[31]	CARC[31]	HSOS[40]	CHIO
S	OA[33]	150[55]	Abc[31]	CADC[31]	11505[+0]	CIIIO

Annual	1,00,589.328	96,647.328	31,910.000	30,596.000	9,533.508	3,623.136
Savings (\$)	0	0	0	0	0	0

Fig. 7 presents the convergence characteristics for all objectives for case 3 and Fig. 8 presents the relative rotor angle deviations after considering the TSC for CHIO and FOX algorithms. We can see that both algorithms were able to maintain transient stability even when the time to clear fault was increased from the maximum clearing time of 0.1298 s by 5.02% to 0.18 s. Maximum RRAD can be seen to lie well below 100° thereby signifying a stable system.

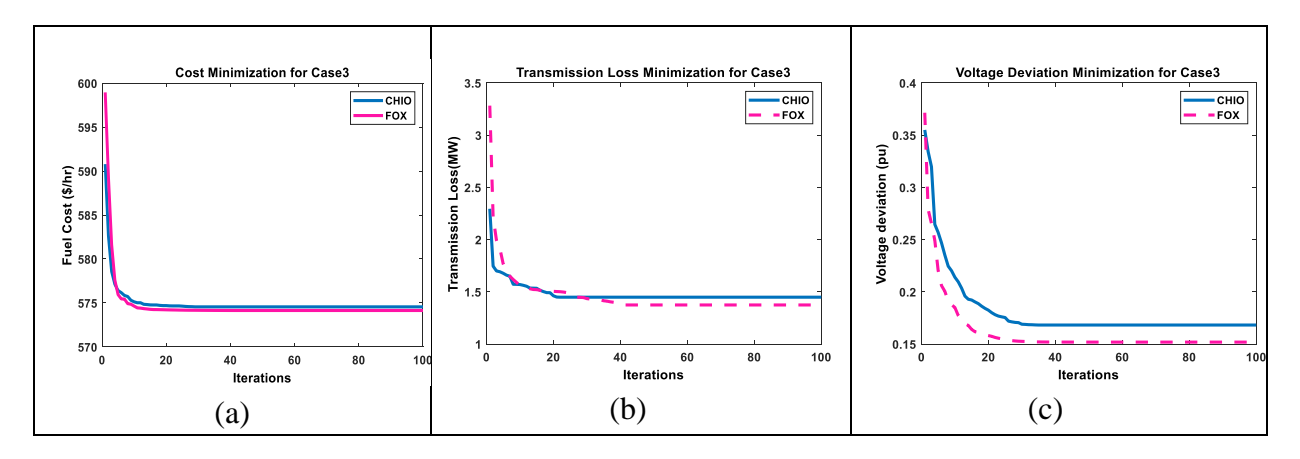
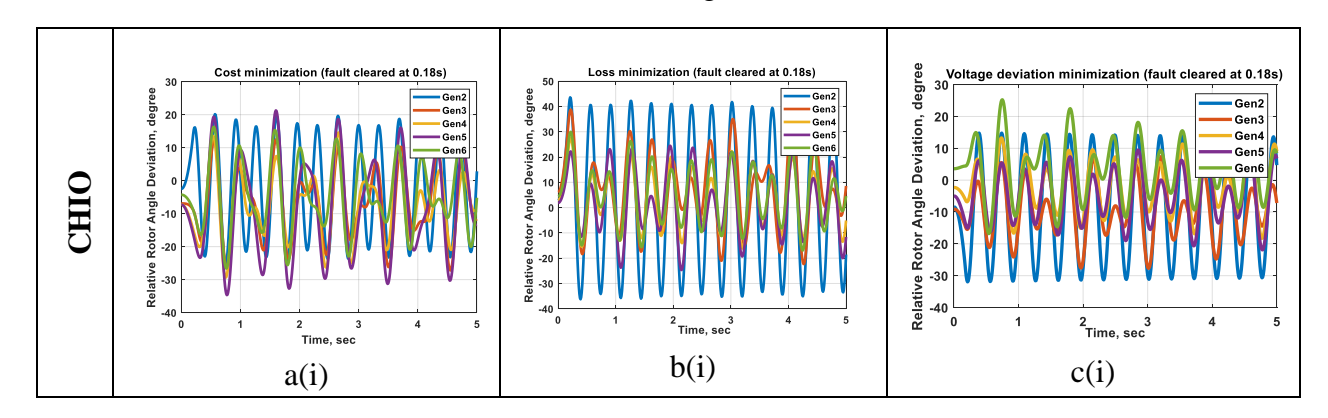


Fig. 7. Convergence characteristics of (a) cost, (b) loss and (c) voltage deviation minimization for Case3 using CHIO and FOX.



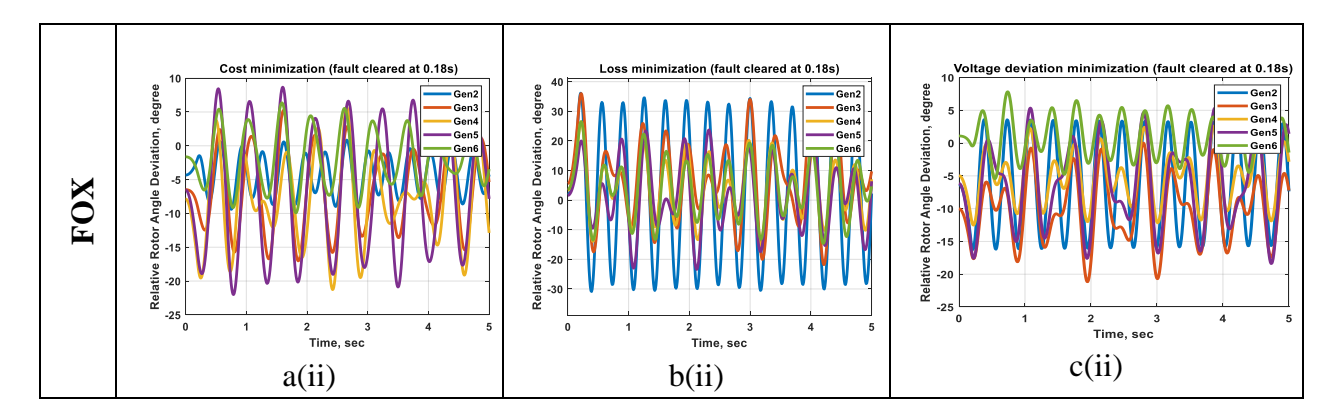


Fig. 8. RRADs for: a(i), a(ii)- cost, b(i), b(ii)- loss, and c(i), c(ii)-voltage deviation minimization, for Case 3 using CHIO and FOX algorithms.

Case4

This is the TSC-POPF case that considered probabilistic generation as mentioned in Case 2 and had to satisfy the TSC of (15). Fault CT is considered to be 0.18 s for this case to check the feasibility of the proposed model. Table 9 presents the control parameters for this case. It can be observed that FOX performed better than CHIO for all objectives.

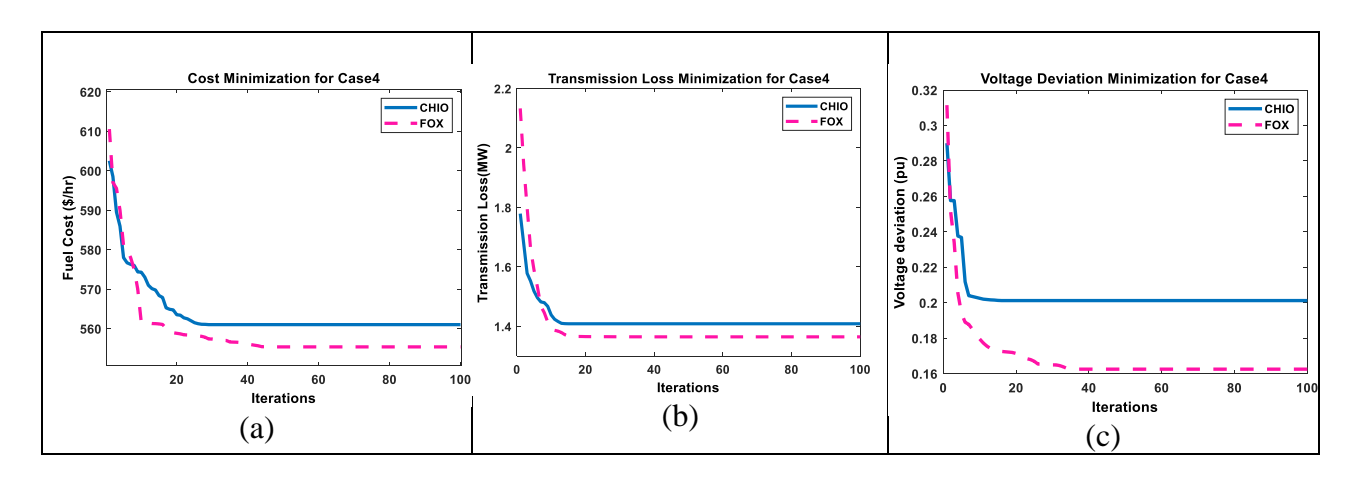


Fig. 9. Convergence characteristics of (a) cost, (b) loss and (c) voltage deviation minimization for Case 4 using CHIO and FOX algorithms.

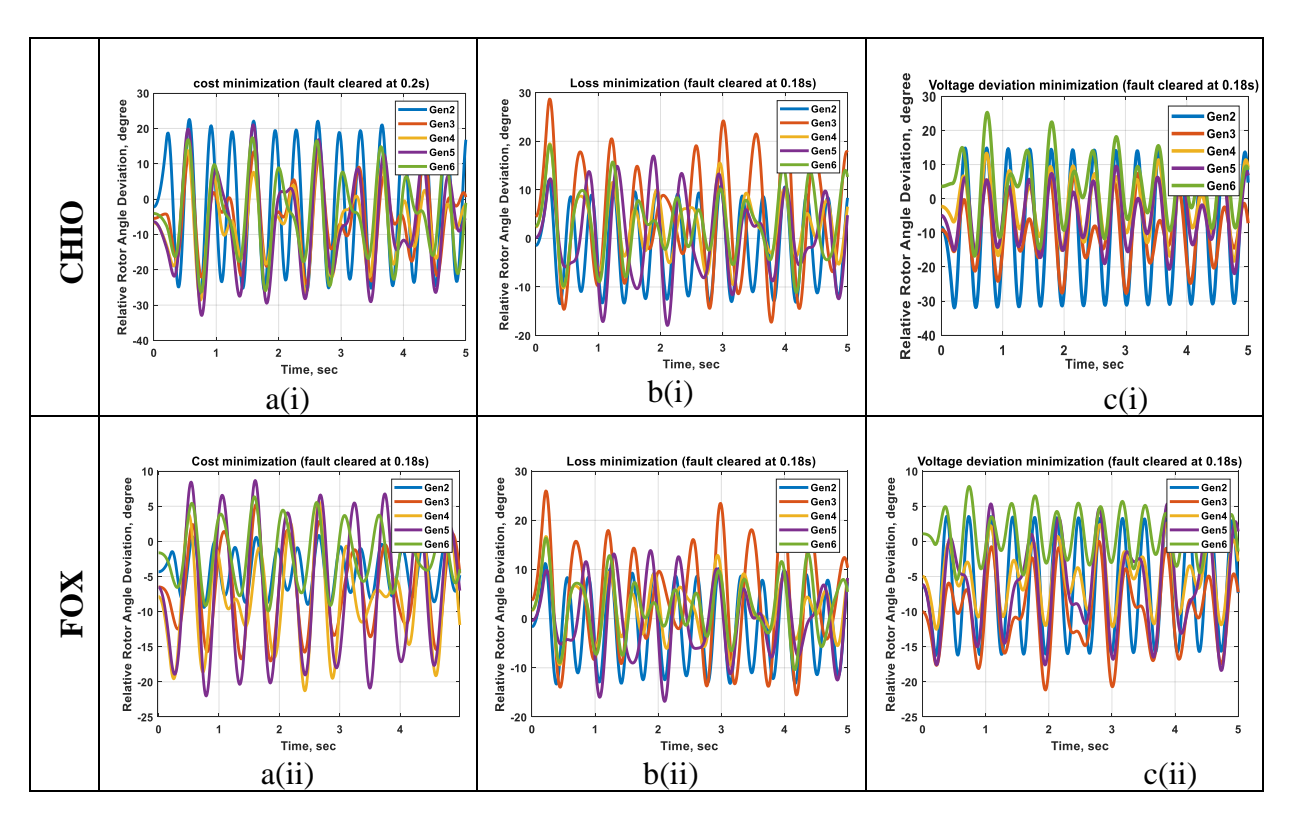


Fig. 10. RRADs for: a(i), a(ii)- cost, b(i), b(ii)- loss, and c(i), c(ii)-voltage deviation minimization, for Case 4 using CHIO and FOX algorithms.

Table 9. Minimmization of all Objectives using CHIO and FOX Algorithms for Case 4.

Corresponding values of	CHIO	FOX	CHIO	FOX	CHIO	FOX
other objectives	Cost		Loss		Voltage Deviation	
Cost(\$/h)	561.0104	555.3704	623.2119	616.7389	636.4246	660.0332
Transmission Loss(MW)	2.3250	2.4130	1.4086	1.3647	5.3008	5.7019
Voltage deviation(p.u.)	0.9032	1.0272	1.5844	1.5379	0.2012	0.1625

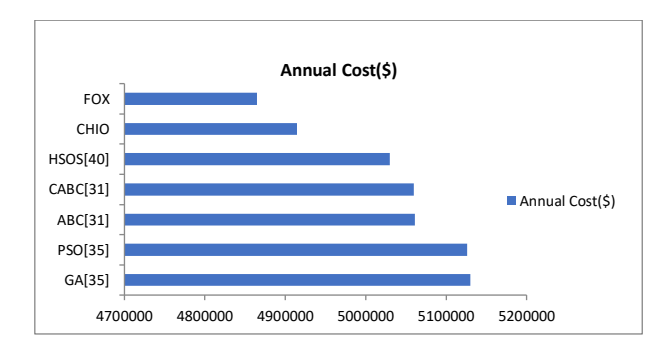


Fig. 11.Comparative annual cost of generation obtained by FOX and CHIO in Case 4 as compared to other algorithms of Case 3.

Algorith ms	GA[38]	PSO[38]	ABC[34]	CABC[34	HSOS	СНІО	FOX
Annual Savings (\$)	2,64,98	2,61,044.	1,96,308.	1,94,994.	1,65,170.	1,68,02	164397
	6.4960	4960	0960	0960	0000	0.30	.17

Table 10. Annual Savings in Generation Cost for Case 5.

Since there are no data reported in the literature to do a comparative study for this case, we compared the results obtained using FOX algorithm with those of Case 3 to detect the annual savings in generation cost and presented them in Table 10. Fig. 9 presents the convergence characteristics of CHIO and FOX. RRADs of this case are depicted in Fig. 10. Fig. 11 represents the annual cost obtained by FOX and CHIO after renewable energy integration as compared to those without renewables in Case 3.

It can be observed from Fig. 10 that transient stability was maintained for all objectives and the maximum RRAD was much below the threshold 150°, which signifies a transiently stable system. From Table 10 and Fig. 11, it is evident that renewable integration to the transient stability constrained system resulted in great annual savings on employing the FOX algorithm.

Case 5

The fault CT was increased to 0.49 s, while all other conditions were kept same as Case 4. Table 11 presents control parameters for this case. We can see that FOX obtained better results for all objectives as compared to CHIO. Also, the annual savings in generation cost as compared to CHIO is 12046.36 \$.

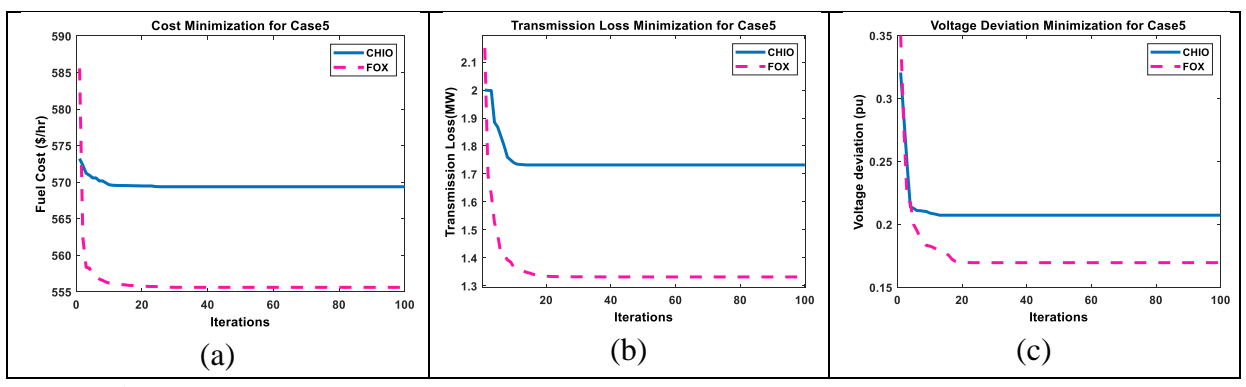
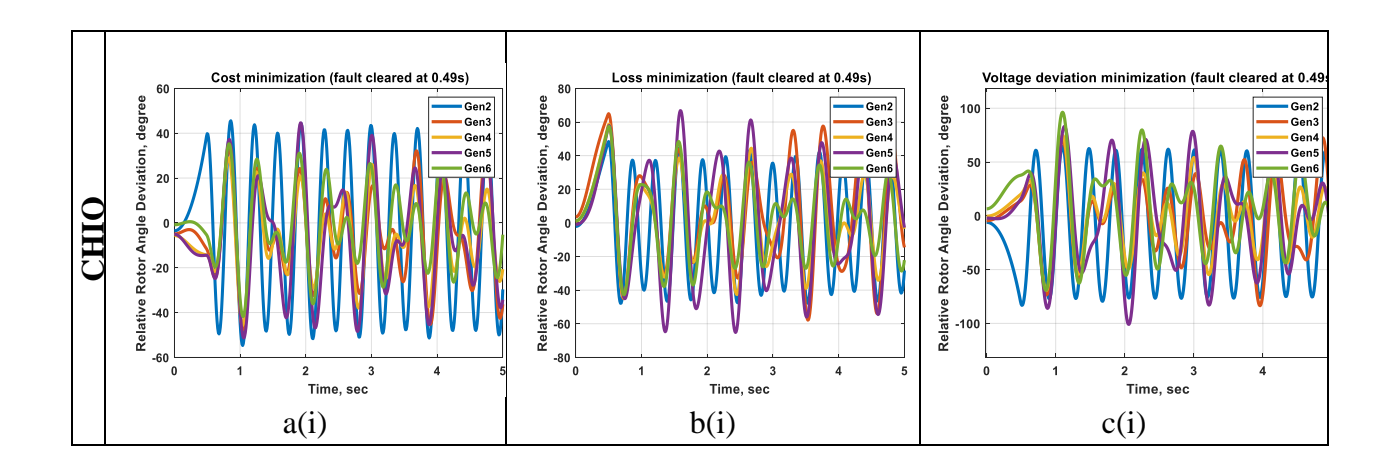


Fig. 12. Convergence characteristics of (a) cost, (b) loss and (c) voltage deviation minimization for Case 5 using CHIO and FOX algorithms.

Table 11. Minimization of all Objectives using CHIO and FOX Algorithms for Case 5.

Corresponding values of	CHIO	FOX	CHIO	FOX	CHIO	FOX
other objectives	Cost		Loss		Voltage Deviation	
Cost(\$/h)	569.371 4	555.610 4	601.413	610.647	627.188 6	637.646
Transmission Loss(MW)	2.3043	2.0725	1.7323	1.3321	5.1380	5.3763
Voltage deviation(p.u.)	0.7407	0.9063	1.7182	1.9853	0.2073	0.1696



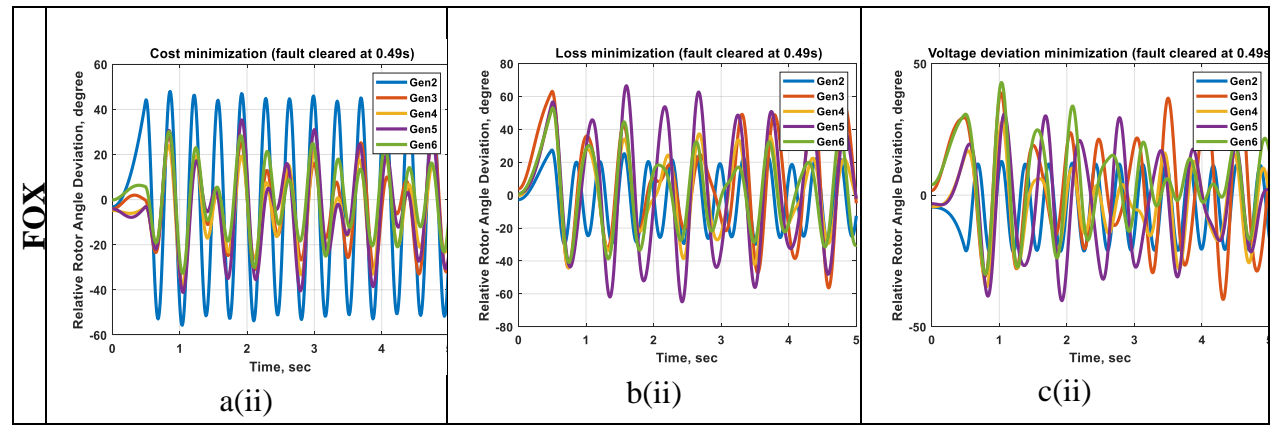


Fig. 13. RRADs for: a(i), a(ii)- cost, b(i), b(ii)- loss, and c(i), c(ii)-voltage deviation minimization, for Case 5 using CHIO and FOX algorithms.

The initial values attained as well as the number of iterations required to converge using FOX algorithm are higher for almost all the cases as compared to CHIO signifying better exploration capability of FOX algorithm over CHIO as evident from Fig. 12. Although, convergence is slightly slower in case of FOX, it is able to deliver better results. It can be a viable option in cases where effect of computation times will not be very significant. Fig. 13 presents the RRADs for an increase in fault CT to 0.49s, which is an increase by 36.02% from the maximum fault CT of 0.1298s. It can be observed that none of the generators are swinging outside the maximum limit of 150°. In fact, the maximum RRAD amongst all objectives was 140° for voltage deviation minimization objective using CHIO while all other RRADs were well below 100°.

Results obtained from the case studies establish feasibility of the proposed TSC-POPF model in ensuring transient stability of the system with sufficient stability margin.

7. Statistical Significance of Test Results

A statistical evaluation is conducted on 50 trial datasets to evaluate the effectiveness of the FOX and CHIO algorithms.

Table 12. Statistical analysis of QRSOS for single objectives using Wilcoxon signed rank test against 50 trials.

					No. of		
					hits to		
	Test			Avera	minimum	Standard	
Algorithm	cases	Minimum	Maximum	ge	solution	deviation	p-value
FOX	case 1	573.1564	573.59	573.28	35	0.2026	1.12E-10

			4	8			
	case2	553.8597	554.92	554.05	41	0.41	3.66E-11
			1	1	41		
	case3	574.1372	574.85	574.28	40	0.2893	4.61E-11
			3	0	40		
	case4	555 2704	555.57	555.41	40	0.002	4.61E-11
		555.3704	5	1	40 0.083	0.083	
	_	555 C104	555.88	555.67	20 0.115	0.1177	6.92E-11
	case5	555.6104	3	6	38	0.1177	
CHIO c	case 1	573.3745	577.48	574.85	32	1.9916	1.57E-10
			2	3	32		
	2	case2 566.3605	570.21	567.36	37	1.71	8.25E-11
	casez		6	3			
	case3	574.5508	577.92	575.96	20	1.6811	1.95E-10
			3	7	29		
	case4	561.0104	563.25	561.77	33	1.073	1.43E-10
			2	3			
	case5	569.3714	572.35	570.20	36	1.3546	9.68E-11
			8	8			

In this analysis, a single sample dataset generated by the proposed algorithm is subjected to the Wilcoxon signed rank test. A p-value, representing the probability value, below 0.05 is interpreted as strong evidence against the null hypothesis.

The resulting p-values from this test for cases 1-5, for cost minimization, along with the corresponding minimum, maximum, average values, and standard deviation, are presented above in Table 12. It is evident that both algorithms exhibited strong and consistent performance, with FOX demonstrating superior results characterized by lower standard deviation and more favourable p-values.

8. Conclusion

This research has introduced a TSC-POPF model, based on the 2m PEM method. The primary objective of this study was to evaluate the practicality and effectiveness of this model in preserving transient stability within a power system, especially in the presence of stochastic renewable energy generation. To address this challenge, two powerful evolutionary algorithms, FOX and CHIO, were harnessed to minimize the objective functions associated with the TSC-POPF problem. A comprehensive set of case studies was meticulously conducted to thoroughly assess the performance of these algorithms under various scenarios. The outcomes of these case studies are promising. They illustrate that the proposed TSC-

POPF model is adept at ensuring transient stability, even when the fault CT is significantly extended. Moreover, the RRAD values observed in these studies consistently fell within the range of 50° to 100°, signifying a substantial margin of stability. This underscores the model's capacity to effectively manage substantial disturbances while upholding a secure level of stability.

To the best of our knowledge, the application of the 2m PEM approach to construct a TSC-POPF model as presented here is unprecedented in the existing literature. This model, when applied, has consistently demonstrated its ability to maintain a robust stability margin in the face of system disturbances. This research advances the understanding and application of TSC-POPF modelling, providing a valuable tool for enhancing the stability and efficiency of power systems incorporating stochastic renewable energy sources. The findings herein contribute to the on-going efforts to create resilient and sustainable power networks in the face of increasing renewable energy integration. It also presents an exhaustive comparative analysis of two very recent evolutionary algorithms FOX and CHIO, in tackling the challenges faced by a power system network.

Statements and Declarations

Acknowledgements

This research is supported by the Ratchadapisek Somphot Fund for Postdoctoral Fellowship and Chulalongkorn University, and Thailand Science Research and Innovation Fund Chulalongkorn University.

Data Availability

Data will be made available on request.

Declaration of competing interests

The authors declare that they have no competing interests to influence the work reported in this paper.

References

- [1] Momoh, A. J., El-Hawary, M. E., & Ramababu, A. (1999). A review of selected optimal power flow literature to 1993. II. Newton, linear programming and interior point methods. IEEE Transactions on Power Systems, 14(1), 105-111.
- [2] Santos, A. Jr., & Da Costa, G. R. M. (1995). Optimal-power-flow solution by Newton's method applied to an augmented Lagrangian function. IEE Proceedings-Generation, Transmission and Distribution, 142(1), 33-36.

- [3] Zhang, S., & Irving, M. R. (1994). Enhanced Newton-Raphson algorithm for normal, controlled and optimal power flow solutions using column exchange techniques. IEE Proceedings-Generation, Transmission and Distribution, 141(6), 647-657.
- [4] Huneault, M., & Galiana, F. D. (1991). A survey of the optimal power flow literature. IEEE Transactions on Power Systems, 6(2), 762-770.
- [5] Burchett, R. C., Happ, H. H., & Vierath, D. R. (No publication date provided). Quadratically convergent optimal power flow. IEEE Transactions on Power Apparatus and Systems, 11, 3267-3275.
- [6] Swain, A. K., & Morris, A. S. (2000). A novel hybrid evolutionary programming method for function optimization. In Proceedings of the 2000 Congress on Evolutionary Computation. CEC00 (Cat. No. 00TH8512) (Vol. 1, pp. 699-705). IEEE.
- [7] Abou El Ela, A. A., Abido, M. A., & Spea, S. R. (2010). Optimal power flow using differential evolution algorithm. Electric Power Systems Research, 80(7), 878-885.
- [8] Abido, M. A. (2002). Optimal power flow using tabu search algorithm. Electric Power Components and Systems, 30(5), 469-483.
- [9] Tripathy, M., & Mishra, S. (2007). Bacteria foraging-based solution to optimize both real power loss and voltage stability limit. IEEE Transactions on Power Systems, 22(1), 240-248.
- [10] Khazali, A. H., & Kalantar, M. (2011). Optimal reactive power dispatch based on harmony search algorithm. International Journal of Electrical Power & Energy Systems, 33(3), 684-692.
- [11] Roy, P. K., Mandal, B., & Bhattacharya, K. (2012). Gravitational search algorithm based optimal reactive power dispatch for voltage stability enhancement. Electric Power Components and Systems, 40(9), 956-976.
- [12] Basu, M. (2014). Teaching-learning-based optimization algorithm for multi-area economic dispatch. Energy, 68, 21-28.
- [13] Abido, M. A. (2011). Multiobjective particle swarm optimization for optimal power flow problem. In Handbook of swarm intelligence (pp. 241-268). Springer.
- [14] Mandal, B., & Roy, P. K. (2014). Multi-objective optimal power flow using quasi-oppositional teaching learning based optimization. Applied Soft Computing, 21, 590-606.
- [15] Roy, P. K., Ghoshal, S. P., & Thakur, S. S. (2010). Multi-objective optimal power flow using biogeography-based optimization. Electric Power Components and Systems, 38(12), 1406-1426.
- [16] Bhattacharya, A., & Chattopadhyay, P. K. (2011). Application of biogeography-based optimisation to solve different optimal power flow problems. IET Generation, Transmission & Distribution, 5(1), 70-80.

- [17] Hernandez, Y. R., & Hiyama, T. (2009). Minimization of voltage deviations, power losses and control actions in a transmission power system. In 2009 15th International Conference on Intelligent System Applications to Power Systems (pp. 1-5). IEEE.
- [18] Swarup, S., & Swarup, K. S. (2011). Multi-objective harmony search algorithm for optimal power flow problem. International Journal of Electrical Power & Energy Systems, 33(3), 745-752.
- [19] Duman, S. (2017). Symbiotic organisms search algorithm for optimal power flow problem based on valve-point effect and prohibited zones. Neural Computing and Applications, 28(11), 3571-3585.
- [20] Von Appen, J., Stetz, T., Braun, M., & Schmiegel, A. (2014). Local voltage control strategies for PV storage systems in distribution grids. IEEE Transactions on Smart Grid, 5(2), 1002-1009.
- [21] Jahangiri, P., & Aliprantis, D. C. (2013). Distributed Volt/VAr control by PV inverters. IEEE Transactions on Power Systems, 28(3), 3429-3439.
- [22] Dall'Anese, E., Dhople, S. V., & Giannakis, G. B. (2014). Optimal dispatch of photovoltaic inverters in residential distribution systems. IEEE Transactions on Sustainable Energy, 5(2), 487-497.
- [23] Samadi, A., Eriksson, R., Söder, L., Rawn, B. G., & Boemer, J. C. (2014). Coordinated active power-dependent voltage regulation in distribution grids with PV systems. IEEE Transactions on Power Delivery, 29(3), 1454-1464.
- [24] Miranda, V., & Saraiva, J. P. (1992). Fuzzy modelling of power system optimal load flow. IEEE Transactions on Power Systems, 7(2), 843-849.
- [25] Zhang, H., & Li, P. (2010). Probabilistic analysis for optimal power flow under uncertainty. IET Generation, Transmission & Distribution, 4(5), 553-561.
- [26] Verbic, G., & Canizares, C. A. (2006). Probabilistic optimal power flow in electricity markets based on a two-point estimate method. IEEE Transactions on Power Systems, 21(4), 1883-1893.
- [27] Schellenberg, A., Rosehart, W., & Aguado, J. (2005). Cumulant-based probabilistic optimal power flow (P-OPF) with Gaussian and gamma distributions. IEEE Transactions on Power Systems, 20(2), 773-781.
- [28] Rosenblueth, E. (1975). Point estimates for probability moments. Proceedings of the National Academy of Sciences, 72(10), 3812-3814.
- [29] Hong, H. P. (1998). An efficient point estimate method for probabilistic analysis. Reliability Engineering & System Safety, 59(3), 261-267.
- [30] Raychaudhuri, S. (2008). Introduction to Monte Carlo simulation. In 2008 Winter simulation conference (pp. 91-100). IEEE.

- [31] Ayan, K., Kılıç, U., & Baraklı, B. (2015). Chaotic artificial bee colony algorithm based solution of security and transient stability constrained optimal power flow. International Journal of Electrical Power & Energy Systems, 64, 136-147.
- [32] Pizano-Martinez, A., Fuerte-Esquivel, C. R., & Ruiz-Vega, D. (2009). Global transient stability-constrained optimal power flow using the SIME method. In 2009 IEEE Power & Energy Society General Meeting (pp. 1-8). IEEE.
- [33] Xu, Y., Dong, Z. Y., Xu, Z., Zhang, R., & Wong, K. P. (2012). Power system transient stability-constrained optimal power flow: A comprehensive review. 2012 IEEE Power and Energy Society General Meeting (pp. 1-7). IEEE.
- [34] Alam, A., & Makram, E. B. (2006). Transient stability constrained optimal power flow. In 2006 IEEE Power Engineering Society General Meeting (pp. 6-pp). IEEE.
- [35] Mo, N., Zou, Z. Y., Chan, K. W., & Pong, T. Y. G. (2007). Transient stability constrained optimal power flow using particle swarm optimization. IET Generation, Transmission & Distribution, 1(3), 476-483.
- [36] Ahmadi, H., Ghasemi, H., Haddadi, A. M., & Lesani, H. (2013). Two approaches to transient stability-constrained optimal power flow. International Journal of Electrical Power & Energy System, 47, 181-192.
- [37] Tu, X., Dessaint, A. L. A., & Kamwa, I. (2014). Fast approach for transient stability constrained optimal power flow based on dynamic reduction method. IET Generation, Transmission & Distribution, 8(7), 1293-1305.
- [38] Mukherjee, A., Roy, P. K., & Mukherjee, V. (2016). Transient stability constrained optimal power flow using oppositional krill herd algorithm. International Journal of Electrical Power & Energy Systems, 83, 283-297.
- [39] Xu, Y., Yang, Y. Z., Dong, K. Meng, J. H. Zhao, and K. P. Wong (2012). A hybrid method for transient stability-constrained optimal power flow computation. IEEE Transactions on Power Systems, 27(4), 1769-1777.
- [40] Saha, A., Bhattacharya, A., Das, P., & Chakraborty, A. K. (2020). HSOS: a novel hybrid algorithm for solving the transient-stability-constrained OPF problem. Soft Computing, 24(10), 7481-7510.
- [41] Prasad, D., Mukherjee, A., & Mukherjee, V. (2017). Transient stability constrained optimal power flow using chaotic whale optimization algorithm. In Handbook of neural computation (pp. 311-332). Academic Press.
- [42] Prasad, D., Mukherjee, A., Shankar, G., & Mukherjee, V. (2017). Application of chaotic whale optimization algorithm for transient stability constrained optimal power flow. IET Science, Measurement & Technology, 11(8), 1002-1013.
- [43] Xia, S., Luo, X., Chan, K. W., Zhou, M., & Li, G. (2016). Probabilistic Transient Stability Constrained Optimal Power Flow for Power Systems With Multiple Correlated

Uncertain Wind Generations. IEEE Transactions on Sustainable Energy, 7(3), 1133-1144.

- [44] Rosenblueth, E. (1981). Two-point estimates in probabilities. Applied Mathematical Modelling, 5(5), 329-335.
- [45] Mohammed, H., & Rashid, T. (2022). FOX: a FOX-inspired optimization algorithm. Applied Intelligence, 1-21.
- [46] Al-Betar, M. A., et al. (2021). Coronavirus herd immunity optimizer (CHIO). Neural Computing and Applications, 33(10), 5011-5042.
- [47] Matpower. (No publication date provided). Case 30: Polish system (Poland, 330 buses). Retrieved from https://matpower.org/docs/ref/matpower5.0/case30.html.
- [48] Zimmerman, R. D., & Murillo-Sanchez, C. E. (2011). Matpower 4.1 user's manual. Power Systems Engineering Research Center (PSERC).
- [49] Červený, J., Begall, S., Koubek, P., Nováková, P., & Burda, H. (2011). Directional preference may enhance hunting accuracy in foraging foxes. Biology Letters, 7(3), 355-357.
- [50] Saha, A., Bhattacharya, A., Das, P., & Chakraborty, A. K. (2019). A novel approach towards uncertainty modeling in multiobjective optimal power flow with renewable integration. International Transactions on Electrical Energy Systems, 29(12), e12136.
- [51] Biswas, P. P., Suganthan, P. N., & Amaratunga, G. A. J. (2017). Optimal power flow solutions incorporating stochastic wind and solar power. Energy Conversion and Management, 148, 1194-1207.
- [52] Biswas, P. P., et al. (2018). Multiobjective economic-environmental power dispatch with stochastic wind-solar-small hydro power. Energy, 150, 1039-1057.
- [53] Wind Turbine Models. Hummer H25.0 (200 kW) Wind Turbine. Retrieved from https://en.wind-turbine-models.com/turbines/1681-hummer-h25.0-200kw#datasheet.